arXiv:1303.6487v1 [hep-ph] 26 Mar 2013

Breit-Wheeler process in very short electromagnetic pulses

A.I. Titov[a,b,c], B. Kämpfer[a,d], H. Takabe[c], and A. Hosaka[e]

[a] *Helmholtz-Zentrum Dresden-Rossendorf, 01314 Dresden, Germany*

[b] *Bogoliubov Laboratory of Theoretical Physics, JINR, Dubna 141980, Russia*

[c] *Institute of Laser Engineering, Yamada-oka, Suita, Osaka 565-0871, Japan*

[d] *Institut für Theoretische Physik, TU Dresden, 01062 Dresden, Germany*

[e] *Research Center of Nuclear Physics,*
10-1 Mihogaoka Ibaraki, 567-0047 Osaka, Japan

Abstract

The generalized Breit-Wheeler process, i.e. the emission of e^+e^- pairs off a probe photon propagating through a polarized short-pulsed electromagnetic (e.g. laser) wave field, is analyzed. We show that the production probability is determined by the interplay of two dynamical effects. The first one is related to the shape and duration of the pulse and the second one is the non-linear dynamics of the interaction of $e^\pm$ with the strong electromagnetic field. The first effect manifests itself most clearly in the weak-field regime, where the small field intensity is compensated by the rapid variation of the electromagnetic field in a limited space-time region, which intensifies the few-photon events and can enhance the production probability by orders of magnitude compared to an infinitely long pulse. Therefore, short pulses may be considered as a powerful amplifier. The non-linear dynamics in the multi-photon Breit-Wheeler regime plays a decisive role at large field intensities, where effects of the pulse shape and duration are less important. In the transition regime, both effects must be taken into account simultaneously. We provide suitable expressions for the e^+e^- production probability for kinematic regions which can be used in transport codes.

PACS numbers: 13.35.Bv, 13.40.Ks, 14.60.Ef

Keywords: Non-linear dynamics, multi-photon effects, sub-threshold processes

I. INTRODUCTION

The rapidly progressing laser technology developments [1] offer opportunities for investigations of quantum systems with short and/or intense pulses [2]. Several fundamental processes of electron-photon interactions in the nonlinear regime thus become accessible. Once these are understood experimentally and theoretically, e.g. within the framework of the standard model of particle physics or plain quantum electrodynamics (QED), one can search for new phenomena hinting also to "new physics". Among the elementary electromagnetic (e.m.) interaction processes is the "conversion of light to matter". Generically, this notion refers to the emergence of particles coupling to the e.m. field. Having in mind electrons (e^-) and positrons (e^+) one is interested in the conversion rate into $e^\pm$, their phase space distributions, the back-reaction on the original e.m. field etc.

Several variants of such conversion processes are known. The linear Breit-Wheeler process [3] $\gamma' + \gamma \to e^+ + e^-$ refers to a perturbative QED process; the generalization to the multi-photon process $\gamma' + n\gamma \to e^+ + e^-$ (nonlinear Breit-Wheeler process) were done in the pioneering work of Reiss [4] as well as Narozhny, Nikishov and Ritus [5, 6]. Attributing theses processes to colliding null fields one can imagine another aspect. In the anti-node of suitably counter propagating e.m. waves an oscillating purely electric field can give rise to the dynamical Schwinger effect [7]; in the low-frequency limit one recovers the famous Schwinger effect [8] awaiting still its experimental verification. These kinds of pair creation processes are related to highly non-perturbative effects [9, 10]. Once pair production is seeded in very intense fields further avalanche like particle production can set in which then could screen the original field or even limit the attainable field strength [11]. One can relate the Breit-Wheeler process to the absorptive part of the probe-photon correlator in an external e.m. field; in our case the latter being a null field too.

In the present paper we focus on colliding null fields in the multi-photon regime and consider the generalized Breit-Wheeler effect for short pulses of e.m. wave fields ranging from weak to high intensities. Phrased differently we analyze e^+e^- pair production by a probe photon γ' traversing a coherent e.m. (i.e. laser) field. The latter one is characterized by the reduced strength

$$\xi^2 = -\frac{e^2\langle A^2\rangle}{M_e^2} \ , \tag{1}$$

where $\langle A^2\rangle$ is the mean square of the e.m. potential, and M_e is the electron mass (we use natural units with $c = \hbar = 1$, $e^2/4\pi = \alpha \approx 1/137.036$). A second relevant dimensionless variable characterizing both null fields is

$$\zeta = \frac{s_{\rm thr}}{s}, \tag{2}$$

where $s_{\rm thr} = 4M_e^2$ and $s = 2\omega\omega'(1 - \cos\Theta_{\vec{k}\vec{k}'})$ (for head-on collision geometry, $\Theta_{\vec{k}\vec{k}'} = \pi$); ω, ω' and $\vec{k}, \vec{k}'$ are the frequencies and three-wave vectors of the laser field and the probe photon, respectively. The variable ζ is a pure kinematic quantity with the meaning that for $\zeta > 1$ the linear Breit-Wheeler process $\gamma' + \gamma \to e^+ + e^-$ is sub-threshold, i.e. kinematically forbidden. However, multi-photon effects enable the non-linear process $\gamma' + n\gamma \to e^+ + e^-$ even for $\zeta > 1$ which we refer to as sub-threshold pair production. The non-linear Breit-Wheeler process has been experimentally verified in the experiment E-144 at SLAC [12]. There, the minimum number of photons involved in one e^+e^- event can be estimated by the integer part of $\zeta(1+\xi^2)$, i.e., five. (To arrive at such an estimate recall that the reduced strength ξ is related to the laser intensity I_L via $\xi^2 \simeq 0.56(\omega(\text{eV}))^{-2}10^{-18}\text{I}_\text{L}/(\text{W/cm}^2)$, and therefore, at $\omega' = 29$ GeV, $\omega = 2.35$ eV, and at peak focused laser intensity of $1.3 \times 10^{18}\,\text{W/cm}^2$, one gets $\xi = 0.36$ and $\zeta = 3.83$. The laser pulses contained about thousand cycles in a shot, allowing to neglect the details of the pulse shape and duration.) A laser intensity of $\sim 2 \times 10^{22}$ W/cm^2 has been already achieved [13]. Intensities of the order of $I_L \sim 10^{23}...10^{25}$ W/cm^2 are envisaged in near future at the CLF [14], ELI [15], and HiPER [16] laser facilities. Such large laser intensities allow for larger values of $\xi^2 \sim I_L$ compared to the SLAC E-144 experiment.

The new generations of optical laser beams are expected to be essentially realized in short pulses (with femtoseconds duration) with only a few oscillations of the e.m. field. High laser intensities are presently achieved by the chirped pulse amplification resulting in short pulses. As shown for the Compton effect in [17–22] and for the Breit-Wheeler effect in [23–26] the pulse shape and the pulse duration become important. That means the treatment of the intense laser field as an infinitely long wave train is no longer adequate. Keeping the spatial plane-wave character we are going to explore here the e^+e^- production as generalized Breit-Wheeler process in finite pulse approximation (FPA), i.e. investigate the impact of the temporal pulse structure, and provide the conditions under which the infinitely long pulse approximation (IPA) can be applied. This problem is of practical interest for the investigation of e^+e^- production in transport Monte Carlo calculations [27, 28], where the probability of pair production in a background field is taken as an input.

We show below that the e^+e^- production probability is determined by the non-trivial interplay of two dynamical effects. The first one is related to the shape and duration of the pulse. The second one is the non-linear dynamics of the $e^\pm$ in the strong electromagnetic field, independently of the pulse geometry. These two effects play quite different roles in two limiting cases: The pulse shape effects manifest most clearly in the weak-field regime characterized by small values of the product $\xi\,\zeta$. The rapid variation of the e.m. field in very short (sub cycle) pulses enhances strongly few-photon events such that their probability may exceed the IPA prediction by orders of magnitude. Non-linear multi-photon dynamics of the strong electromagnetic field plays a dominant role at large values of ξ^2. In the transition region, i.e. at intermediate values $\xi^2 \sim 1$, the pair creation probability is determined by the interplay of both effects which must be taken into account simultaneously.

Our paper is organized as follows. In Sect. II we derive the basic expressions for the probability of e^+e^- creation in FPA and consider a few prototypical pulse envelope shapes. In Sect. III we discuss the case of ultra-short (sub cycle) pulses where the number of oscillations of the laser field is smaller than one. The case of short pulses with a few oscillations of the laser field within one pulse is considered in Sect. IV. In particular, we analyze the enhancement of the production probability in the sub-threshold region at small values of ξ^2, discuss the case of intermediate $\xi^2 \sim 1$, and evaluate the production probability at large values of ξ^2. Our conclusions are given in Sect. V. In Appendix A, for completeness and easy reference, we present some details of the derivation of the production probability for very high intensities, $\xi^2 \gg 1$.

II. ELECTRON-POSITRON EMISSION IN A SHORT PULSE

A. General formalism

In the following we employ the e.m. four-potential of the circularly polarized laser field in the axial gauge $A^\mu = (0,\,\vec{A}(\phi))$ with

$$\vec{A}(\phi) = f(\phi)\left(\vec{a}_x \cos(\phi + \hat{\phi}) + \vec{a}_y \sin(\phi + \hat{\phi})\right)\ , \tag{3}$$

where $\phi = k\cdot x$ is invariant phase with four-wave vector $k = (\omega, \vec{k})$, obeying the null field property $k^2 = k\cdot k = 0$ (a dot between four-vectors indicates the Lorentz scalar product); $\hat{\phi}$

is the carrier envelope phase; $|\vec{a}_x|^2 = |\vec{a}_y|^2 = a^2$, $\vec{a}_x\vec{a}_y = 0$. Transversality means $\vec{k}\vec{a}_{x,y} = 0$ in the present gauge. Instead switching on/off the periodic e.m. field we encode the finiteness of a pulse in the envelope function $f(\phi)$ with $\lim\limits_{\phi\to\pm\infty} f(\phi) = 0$ (FPA). To characterize the pulse duration one may use the number N of cycles in a pulse, $N = \Delta/\pi = \frac{1}{2}\tau\omega$, where the dimensionless quantity Δ or the duration of the pulse τ are further useful measures. Below we analyze the dependence of observables on the shape of $f(\phi)$ for a variety of relevant envelopes. The IPA case is defined by $f(\phi) = 1$. The carrier envelope phase $\hat{\phi}$ is particularly important if it is comparable with the pulse duration Δ. In IPA it is anyhow irrelevant; in FPA with $\hat{\phi} \simeq \Delta$ the production probability would be determined by an involved interplay of the carrier phase, the pulse duration and pulse shape as well as the parameters ξ and ζ as emphasized, e.g., in [25, 29, 30]. In present work, we drop the carrier phase, thus assuming $\hat{\phi} \ll \Delta$, and concentrate on the dependence of the production probability on the parameters ξ and ζ together with pulse shape and pulse duration. A detailed analysis of the impact of $\hat{\phi}$ on the pair production needs a separate investigation which is postponed to subsequent work.

Utilization of the e.m. potential of (3) leads to two significant modifications of the transition amplitude in FPA compared to IPA. In IPA, the Volkov solutions [31, 32] refer to Fermions with quasi-momenta and dressed masses. In FPA, all in- and out- momenta and masses take their vacuum values. The finite (in space-time) e.m. potential (3) for FPA requires the use of Fourier integrals for invariant amplitudes, instead of Fourier series which are employed in IPA. The partial harmonics become thus continuously in FPA. The S matrix element is expressed generically as

$$S_{fi} = \frac{-ie}{\sqrt{2p_0 2p'_0 2\omega'}} \int\limits_{\zeta}^{\infty} dl\, M_{fi}(l)(2\pi)^4\delta^4(k' + lk - p - p'), \tag{4}$$

where k, k', p and p' refer to the four-momenta of the background (laser) field (3), incoming probe photon, outgoing positron and electron, respectively. The transition matrix $M_{fi}(l)$, similarly to the case of the non-linear Compton effect [17, 19–21], consists of four terms

$$M_{fi}(l) = \sum_{i=0}^{3} M^{(i)}\, C^{(i)}(l)\ , \tag{5}$$

where

$$
\begin{aligned}
C^{(0)}(l) &= \frac{1}{2\pi}\int\limits_{-\infty}^{\infty} d\phi\, \mathrm{e}^{il\phi - i\mathcal{P}(\phi)} \ , \\
C^{(1)}(l) &= \frac{1}{2\pi}\int\limits_{-\infty}^{\infty} d\phi f^2(\phi)\, \mathrm{e}^{il\phi - i\mathcal{P}(\phi)} \ , \\
C^{(2)}(l) &= \frac{1}{2\pi}\int\limits_{-\infty}^{\infty} d\phi f(\phi)\, \cos\phi\, \mathrm{e}^{il\phi - i\mathcal{P}(\phi)} \ , \\
C^{(3)}(l) &= \frac{1}{2\pi}\int\limits_{-\infty}^{\infty} d\phi f(\phi)\, \sin\phi\, \mathrm{e}^{il\phi - i\mathcal{P}(\phi)} \ , \qquad (6)
\end{aligned}
$$

with

$$
\mathcal{P}(\phi) = z\int\limits_{-\infty}^{\phi} d\phi'\, \cos(\phi' - \phi_0) f(\phi') - \xi^2\zeta u \int\limits_{-\infty}^{\phi} d\phi'\, f^2(\phi') \ . \qquad (7)
$$

The quantity z is related to ξ, l, $u \equiv (k'\cdot k)^2/\left(4(k\cdot p)(k\cdot p')\right)$, and $u_l \equiv l/\zeta$ via

$$
z = 2l\xi\sqrt{\frac{u}{u_l}\left(1 - \frac{u}{u_l}\right)} \ . \qquad (8)
$$

The phase ϕ_0 is equal to the azimuthal angle of the electron emission direction in the e^+e^- pair rest frame $\phi_{p'}$ and is related to the azimuthal angle of the positron as $\phi_0 = \phi_p + \pi$. Similarly to IPA, it can be determined through invariants $\alpha_{1,2}$ as $\cos\phi_0 = \alpha_1/z$, $\sin\phi_0 = \alpha_2/z$ with $\alpha_{1,2} = e\left(a_{1,2}\cdot p/k\cdot p - a_{1,2}\cdot p'/k\cdot p'\right)$.

The transition operators $M^{(i)}$ in Eq. (5) have the form

$$
M^{(i)} = \bar{u}_{p'}\, \hat{M}^{(i)}\, v_p \qquad (9)
$$

with

$$
\begin{aligned}
\hat{M}^{(0)} &= \not{\varepsilon}' \ , \qquad \hat{M}^{(1)} = \frac{e^2(\not{a}_1\, \not{k}\not{\varepsilon}'\, \not{k}\not{a}_1 + \not{a}_2\, \not{k}\not{\varepsilon}'\, \not{k}\not{a}_2)}{4(k\cdot p)(k\cdot p')} \ , \\
\hat{M}^{(2)} &= \frac{e\not{a}_1\not{k}\not{\varepsilon}'}{2(k\cdot p')} + \frac{e\not{\varepsilon}'\not{k}\not{a}_1}{2(k\cdot p)} \ , \qquad \hat{M}^{(3)} = \frac{e\not{a}_2\not{k}\not{\varepsilon}'}{2(k\cdot p)} + \frac{e\not{\varepsilon}'\not{k}\not{a}_2}{2(k\cdot p')} \ , \qquad (10)
\end{aligned}
$$

where u and v are Dirac spinors of the electron and positron, respectively, and ε' is the polarization four-vector of the probe photon.

The integrand of the function $C^{(0)}$ does not contain the envelope function $f(\phi)$ and therefore it is divergent. One can regularize it by using the prescription of Ref. [17]. The formal result

$$C^{(0)}(l) = \frac{1}{2\pi l}\int\limits_{-\infty}^{\infty} d\phi\left(z\cos(\phi-\phi_0)\,f(\phi) - \xi^2\zeta u\,f^2(\phi)\right)\,\mathrm{e}^{il\phi - i\mathcal{P}(\phi)} + \delta(l)\,\mathrm{e}^{-i\mathcal{P}(0)} \tag{11}$$

contains a singular term (last term) which however does not contribute because of kinematical considerations implying $l > 0$. The differential probability of e^+e^- pair production in terms of the transition matrix $M_{fi}(l)$ in Eq. (4) reads

$$dW = \frac{\alpha\zeta^{1/2}}{2\pi N_0 M_e}\int\limits_{\zeta}^{\infty} dl\;|M_{fi}(l)|^2\,\frac{d\vec{p}}{2p_0}\,\frac{d\vec{p}'}{2p_0'}\delta^4(k' + lk - p - p')\ . \tag{12}$$

It may be represented in conventional form as a function of u and ϕ_p

$$\frac{dW}{d\phi_p\,du} = \frac{\alpha M_e\zeta^{1/2}}{16\pi N_0}\,\frac{1}{u^{3/2}\sqrt{u-1}}\int\limits_{\zeta}^{\infty} dl\;w(l) \tag{13}$$

with

$$\begin{aligned}\frac{1}{2}\,w(l) \;&=\; (2u_l+1)|C^{(0)}(l)|^2 + \xi^2(2u-1)(|C^{(2)}(l)|^2 + |C^{(3)}(l)|^2)\\ &+\; \mathrm{Re}\,C^{(0)}(l)\left(\xi^2 C^{(1)}(l) - \frac{2z}{\zeta}(\alpha_1 C^{(2)}(l) + \alpha_2 C^{(3)}(l))\right)^*\ .\end{aligned} \tag{14}$$

The differential probability dW in Eq. (13), in fact is the probability per unit time (or rate). The time units in IPA ($\Delta T^{(IPA)}$) and FPA ($\Delta T^{(FPA)}$) are different. The ratio of $N_0 \equiv \Delta T^{(IPA)}/\Delta T^{(FPA)}$ may be evaluated as following. The variation of e.m. energy of a pulse in a volume $\int_{-\infty}^{\infty} S\,dz$, where S is an unit cross section in the $x-y$ plane, per $\Delta T^{(FPA)}$ is equal to the integral of the energy flux vector for the electromagnetic energy $\vec{I}$ (Poynting vector) over the area $\oint_s d\vec{S}\,\vec{I}$. Taking into account that this integral is the same in FPA and IPA one finds

$$N_0 = \frac{\int\limits_{-\infty}^{\infty} S\,dz\,(\mathbf{E}^2_{FPA} + \mathbf{B}^2_{FPA})}{\int\limits_{0}^{\lambda} S\,dz\,(\mathbf{E}^2_{IPA} + \mathbf{B}^2_{IPA})} = \frac{1}{2\pi}\int\limits_{-\infty}^{\infty} d\phi\,(f^2(\phi) + f^{'2}(\phi)), \tag{15}$$

where $\lambda = 2\pi/\omega$ is the wave length, and $\mathbf{E} = -\frac{\partial\mathbf{A}}{dt}$ and $\mathbf{B} = \nabla\times\mathbf{A}$ are electric and magnetic fields, respectively. For a convenient comparison of IPA and FPA results, the latter one is scaled in Eq. (13) by $1/N_0$. For IPA, $N_0 = 1$.

B. Envelope functions

We consider one-parameter and two-parameter envelope functions. Among the one-parameter functions we choose the hyperbolic secant (hs) and Gaussian (G) pulses [20, 23]

$$f_{\rm hs}(\phi) = \frac{1}{\cosh\frac{\phi}{\Delta}} \;, \qquad f_{\rm G}(\phi) = \exp\left[-\frac{\phi^2}{2\tau_{\rm G}^2}\right] \;. \tag{16}$$

As the two-parameter function, we choose the symmetrized Fermi (sF) shape [33]

$$f_{\rm sF}(\phi) = \frac{\cosh\frac{\tau_{\rm sF}}{b} + 1}{\cosh\frac{\tau_{\rm sF}}{b} + \cosh\frac{\phi}{b}} \;. \tag{17}$$

The scale parameters Δ, $\tau_{\rm G}$ and $\tau_{\rm sF}$ determine the normalization factor N_0 in (15): $N_{\rm hs} = \frac{\Delta}{\pi}\left(1 + \frac{1}{3\Delta^2}\right)$, $N_{\rm G} = \frac{\tau_{\rm G}}{2\sqrt{\pi}}\left(1 + \frac{1}{2\tau_{\rm G}^2}\right)$, and $N_{\rm sF} = \frac{b}{\pi}\left(F_1\left(t\right)\log\frac{1+\exp[\tau_{\rm sF}/b]}{1+\exp[-\tau_{\rm sF}/b]} + F_2\left(t\right)\right)$ with $t = (\cosh\frac{\tau_{\rm sF}}{b} + 1)/\sinh\frac{\tau_{\rm sF}}{b}$. In the latter case we have defined $F_1(t) = (t^2+1)(-t^4+10t^2-1)/16t$ and $F_2(t) = \left(3t^{10} - 35t^8 + 90t^6 - 90t^4 + 35t^2 - 3\right)/(24(t^2-1)^3)$. In the limit of small $b/\tau_{\rm sF} \to 0$, one finds $N_{\rm sF} = \frac{\tau_{\rm sF}}{\pi}\left(1 - \frac{5}{6}\frac{b}{\tau_{\rm sF}}\right) + \mathcal{O}\left(\exp\left[-\frac{\tau_{\rm sF}}{b}\right]\right)$.

For large Δ and $\tau_{\rm sF}$, and small $b/\tau_{\rm sF} \ll 1$, one can find $N_{\rm sF} \simeq N_{\rm hs}$ at $\tau_{\rm sF} = \Delta$. Therefore, for the sake of comparison we denote $N_0 = N_{\rm hs}$, $\tau_{sF} = \Delta$ and choose the ratio b/Δ as an independent parameter, which determines in turn the normalization factor $N_{\rm sF}$ at finite values of b/Δ.

The scale parameters Δ and $\tau_{\rm G}$ are related to each other by $\tau_{\rm G} = \sqrt{\pi}N_0\left(1 + \sqrt{1 - \frac{1}{2\pi N_0^2}}\right)$ for the fixed normalization factors $N_0 = N_G = N_{\rm hs}$.

The one- and two-parameter envelope functions are exhibited at the left and right panels of Fig. 1. Top panels depict to the envelope functions $f(\phi)$, the middle and bottom panels depict the product $f(\phi)\cos\phi$, which determines the function $\mathcal{P}$ in Eq. (7). The top and the middle panels are for an ultra-short pulse (sub cycle) with the number of oscillations less than one, $N = 0.5$. The bottom panels correspond to a short pulse with $N = 5$. One-parameter envelopes are similar to each other and are close to the two-parameter envelope with $b/\Delta \simeq 0.5$. Decreasing b/Δ results in an essential modification of the envelope function $f(\phi)$: it becomes close to the flat-top profile with the double step shape $\theta(\Delta^2 - \phi^2)$.

III. ULTRA-SHORT PULSES

In this section we consider the pair production due to interaction of the probe photon with an ultra-short pulse, where the number of cycles less than one.

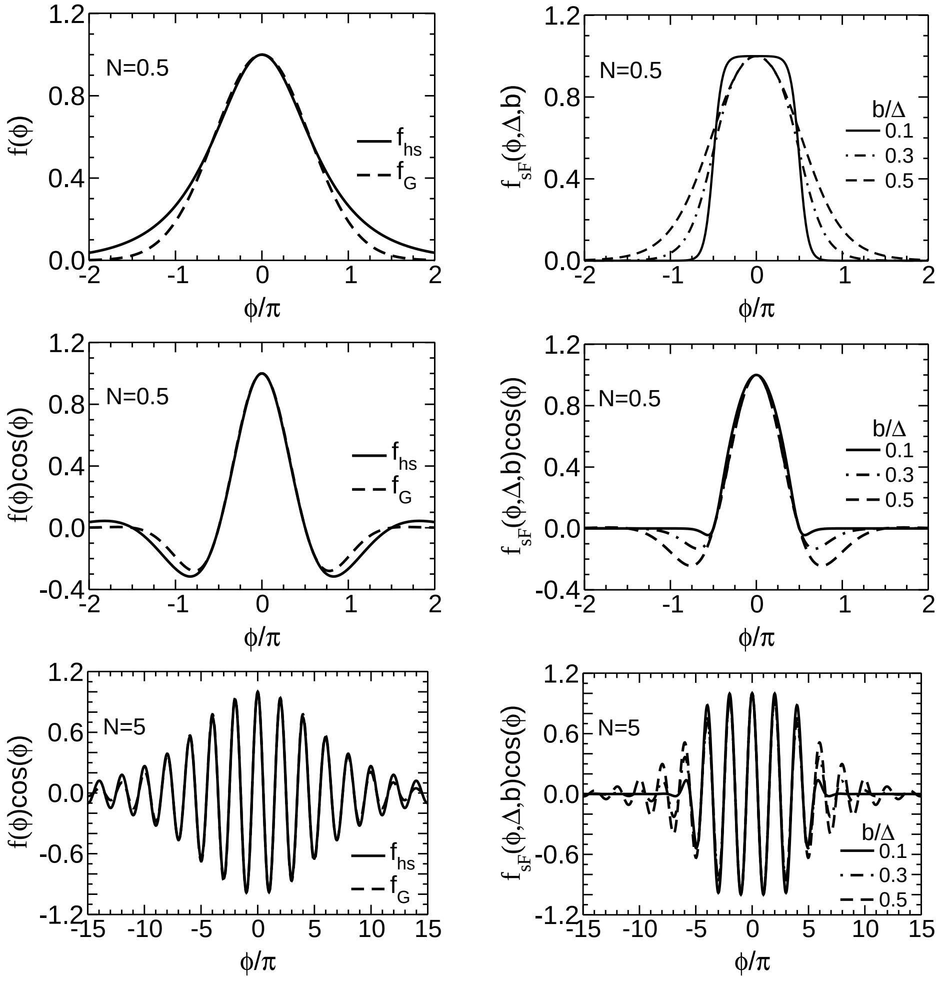

FIG. 1: Pulse envelope $f(\phi)$ (top panels) and the product $f(\phi)\cos\phi$ (middle and bottom panels) as a function of the invariant phase ϕ. The left and right panels correspond to the one- and two-parameter envelope functions, respectively. The top and the middle panels exhibit an ultra-short pulse with the number of oscillations less than one, $N = 0.5$, while the bottom panels are for a short pulse with $N = 5$.

A. The case of small field intensity ($\xi^2 \ll 1$)

Consider first the case of small field intensities and a finite sub-threshold parameter ζ characterized by the relations $z \ll 1$ or $\xi\zeta \ll 1$.

The basic functions $C^{(i)}(l)$ in Eqs. (6) and (14) can be expressed in this regime as a superposition of the functions

$$\mathcal{Y}(l) = \frac{1}{2\pi}\int\limits_{-\infty}^{\infty} d\phi\, \mathrm{e}^{il\phi}\, f(\phi)\, g(\phi) = \int\limits_{-\infty}^{\infty} dq\, F(l-q)\, G(q)\ , \tag{18}$$

where $F(p)$ and $G(q)$ are the Fourier transforms of the envelope function $f(\phi)$ and the function $g(\phi) = \exp\left[-i\mathcal{P}(\phi)\right]$, respectively: $F(p) = \frac{1}{2\pi}\int\limits_{-\infty}^{\infty} d\phi\, \mathrm{e}^{ip\phi}\, f(\phi)$, $G(q) = \frac{1}{2\pi}\int\limits_{-\infty}^{\infty} d\phi\, \mathrm{e}^{iq\phi}\, g(\phi)$. For small values of z, $z \ll 1$, $G(q) \simeq \delta(q - q_0)$, where $q_0 \simeq \langle \mathcal{P}'_\phi \rangle$ with $q_0 \sim \xi\zeta \ll 1$, and $\mathcal{Y}(l) \simeq F(l)$. Keeping the leading terms in Eq. (14) with $C^{(i)} \simeq \mathcal{Y}(l-1) \simeq F(l-1)$, one can obtain an approximate expression for the total production probability:

$$W = \alpha M_e \zeta^{1/2} \xi^2 \int\limits_{\zeta}^{\infty} dl \Phi(l)\, F^2(l-1)\ , \tag{19}$$

with

$$\Phi(l) = v \int\limits_{0}^{1} d\cos\theta \left(\frac{u}{u_l} - \frac{u^2}{u_l^2} + u - \frac{1}{2} \right)\ , \tag{20}$$

where $u = 1/(1 - v^2\cos^2\theta)$; θ and v are the polar angle and the velocity of the outgoing positron in the e^+e^- c.m.s., respectively: $v = \sqrt{1 - \zeta/l}$. An explicit calculation results in

$$\Phi(l) = \frac{1}{2}\left\{ \left(1 + \frac{\zeta}{l} - \frac{\zeta^2}{2l^2}\right) \log\frac{1+v}{1-v} - v\left(1 + \frac{\zeta}{l}\right) \right\}\ . \tag{21}$$

The Fourier transforms of the envelope functions (16) and (17) read

$$\begin{aligned} F_{\rm hs}(l) &= \frac{\Delta}{2\cosh\frac{1}{2}\pi\Delta l}\ , \\ F_{\rm G}(l) &= \frac{\tau_{\rm G}}{\sqrt{2\pi}} \exp\left[-\frac{1}{2}\tau_{\rm G}^2 l^2\right]\ , \\ F_{\rm sF}(l) &= \frac{1 + \exp\left[-\frac{\Delta}{b}\right]}{1 - \exp\left[-\frac{\Delta}{b}\right]} \frac{b\, \sin\Delta l}{\sinh\pi b l}\ . \end{aligned} \tag{22}$$

The square of the Fourier transforms of the envelope functions for a sub cycle pulse with $N = 0.5$ are presented in Fig. 2. On the left panel, the solid and dashed curves correspond to the hyperbolic secant and Gaussian shapes, respectively. One can see a fast monotonic decrease of both the functions with some enhancement of $F_{\rm hs}$ at large values of l. The square of the Fourier transform for the symmetrized Fermi shape is shown in the right panel, where the solid, dot-dashed and dashed curves correspond to the ratios $b/\Delta = 0.1$, 0.3, and 0.5, respectively. One can see large qualitative and quantitative differences between the one-parameter and symmetrized Fermi shapes, in particularly, at $b/\Delta \le 0.3$. In the second case, F^2 decreases exponentially as $\exp\left[-2\pi\Delta\frac{b}{\Delta}\right]$. The slope decreases proportionally to b/Δ (at fixed Δ). Also, the function oscillates with the period $\delta\, l = \pi/\Delta = \pi/0.5\pi = 2$. Contrary

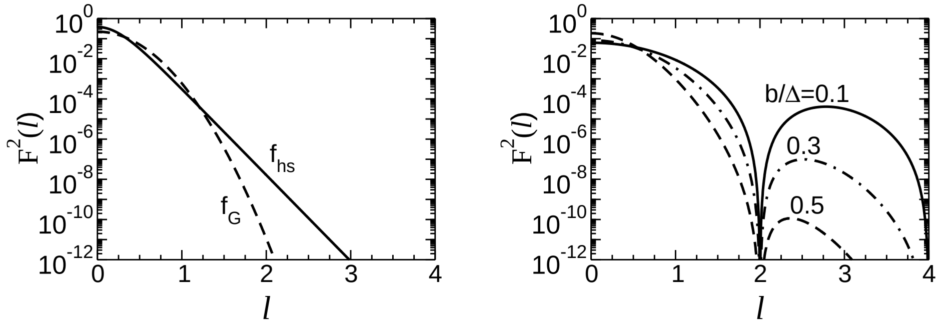

FIG. 2: Square of the Fourier transforms of envelope functions for a sub cycle pulse with $N = 0.5$. Left panel: The solid and dashed curves depict the hyperbolic secant and Gaussian shapes, respectively. Right panel: The solid, dot-dashed and dashed curves show the symmetrized Fermi shape for $b/\Delta = 0.1$, 0.3, and 0.5, respectively.

to the above one-parameter shapes, the function $F_{\rm sF}$ has a significant high-l component at $2 \leq l \leq 4$. This strong effect is not seen in the ϕ-space (cf. Fig. 1, top panels), where all envelope functions look similar to each other. However, the differences in l-space are very important for the pair production.

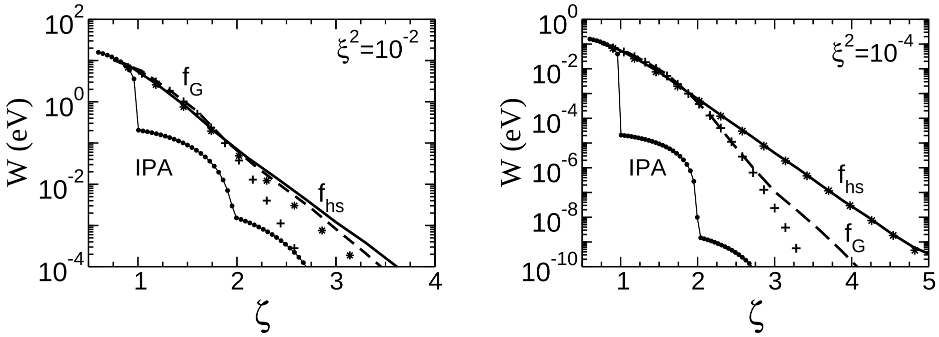

FIG. 3: The probability W of e^+e^- production as a function of the sub-threshold parameter ζ for one-parameter envelope functions for an ultra-short pulse with $N = 0.5$. The solid and dashed curves correspond to numerical calculations with the hyperbolic secant and Gaussian shapes, respectively. The symbols "star" and "plus" are for the approximation (19). The thin solid curves marked by dots correspond to IPA. The left and right panels are for $\xi^2 = 10^{-2}$ and 10^{-4}, respectively.

Our prediction for the total probability of e^+e^- pair production as a function of the sub-threshold parameter ζ for the one-parameter envelope functions for an ultra-short pulse with $N = 0.5$ is shown in Fig. 3. The solid and dashed curves exhibit results of numerical calculations using Eq. (13) with the hyperbolic secant and Gaussian shapes, respectively. The symbols ”star” and ”plus” display the resultsobtained by using the approximation (19). The thin solid curves marked by dots correspond to the IPA case. The left and right panels display results for $\xi^2 = 10^{-2}$ and 10^{-4}, respectively. One can see an agreement of predictions for the ultra-short pulse and IPA near and above the threshold at $\zeta \lesssim 1$, and a strong difference between them below the threshold, i.e. for $\zeta > 1$. Our approximate (analytical) solution of Eq. (19) is in a fairly well agreement with the complete numerical calculation. The function $\Phi(l)$ in Eq. (19) is rather smooth compared to the Fourier transform $F(l-1)$, therefore, the dominant contribution to the integral in Eq. (19) comes from the lower limit of l and, qualitatively, the slope of the probability as a function of ζ is determined by the scale parameters of the envelope functions

$$W_{\rm hs}(\zeta) \sim \exp\left[-\pi\Delta\zeta\right] \ , \qquad W_{\rm G}(\zeta) \sim \exp\left[-\tau_{\rm G}^2\zeta^2\right] \ . \tag{23}$$

Despite of the exponential decrease of the probability W as a function of ζ, one can see a large difference (several orders of magnitude) between predictions for the ultra-short pulse and IPA (or ”crossed field approximation”). In the latter case the probability decreases much faster with increasing ζ.

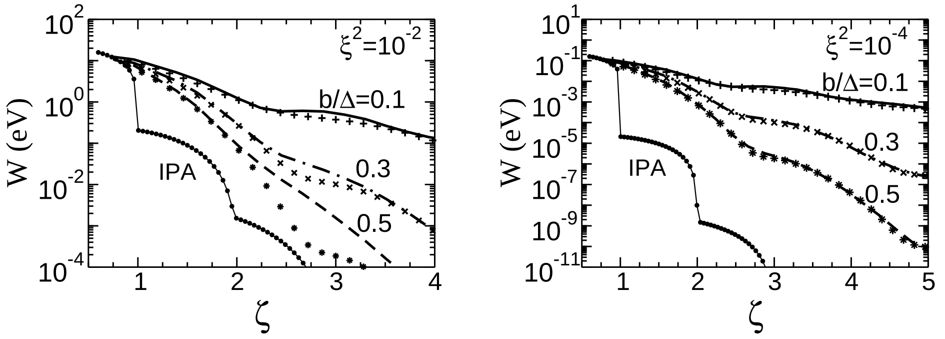

FIG. 4: The same as in Fig. 3 but for symmetrized Fermi shape envelope. The solid, dot-dashed and dashed are for $b/\Delta = 0.1$, 0.3 and 0.5, respectively. The corresponding approximate solutions are shown by symbols ”+”, ”x” and ”$*$”, respectively.

Our results for the symmetrized Fermi envelope is presented in Fig. 4. Now, the shape of the probability is determined by the two parameters b (or b/Δ) and Δ

$$W_{\rm sf}(\zeta) \sim \exp\left[-2\pi\Delta\frac{b}{\Delta}\zeta\right]\sin^2\Delta\zeta \ . \tag{24}$$

The first term describes the slope of the probability as a function of ζ. The slope is proportional to the ”ramping time” of the envelope function, b (or to the ratio $b/Delta$ at fixed Δ). The second term, following from the Fourier transform shown in Fig. 2, describes some oscillations with a period inversely proportional to the duration Δ of the flat-top section; it is independent of the ramping parameter b. Again, one can see a great difference between predictions for the ultra-short pulse and IPA on qualitative and quantitative levels. The probability in IPA has a typical step-like behavior, where each new step indicates the contribution of the next integer harmonic. In FPA, the probability decreases monotonically with a slope determined by the shape of the envelope. The quantitative difference is rather large and, as predicted by results shown in Figs. 3 and 4, can reach orders of magnitude depending on the shape of the envelope(s).

B. Anisotropy

As we have shown above, at small values of z, $z \ll 1$, the probability of e^+e^- production is essentially determined by the pulse shape. The function $g(\phi)$ in Eq. (18) is not important and, therefore, the total probability would be isotropic with respect to the azimuthal angle $\phi_{e^-} = \phi_0$ because only the function $\mathcal{P}(\phi)$ contains a ϕ_0-dependence. For finite values of z, the function $g(\phi)$ becomes important, and the electron (positron) azimuthal angle distribution is anisotropic relative to the direction of the vector $\vec{a}_x$ in Eq. (3), at least for the monotonically rapidly decreasing one-parameter envelope shapes. The reason of an anisotropy is the following. At finite values of z, the function $Y(l)$ in Eq. (18) is determined by the integral over $d\phi$ with a rapidly oscillating function proportional to the exponential

$$\mathrm{e}^{i\left[l\phi - z\left(\cos\phi_0 \int\limits_{-\infty}^{\phi} d\phi'\, f(\phi')\cos\phi' + \sin\phi_0 \int\limits_{-\infty}^{\phi} d\phi'\, f(\phi')\sin\phi'\right)\right]}\,. \tag{25}$$

In case of a fast-decreasing function $f(\phi')$, the contribution of the term proportional to $\sin\phi_0$ is much smaller compared to the term proportional to $\cos\phi_0$. At finite z, the dominant contribution to the functions $\mathcal{Y}(l)$ comes from the region where the difference in the exponent is minimal, i.e. $\phi_e = \phi_0 \simeq 0$. This means that the electrons would be emitted mostly along the vector $\vec{a}_x$ and the positrons in the opposite direction.

We define the anisotropy of the electron emission by

$$\mathcal{A} = \frac{dW(\phi_e) - dW(\phi_e + \pi)}{dW(\phi_e) + dW(\phi_e + \pi)}\,. \tag{26}$$

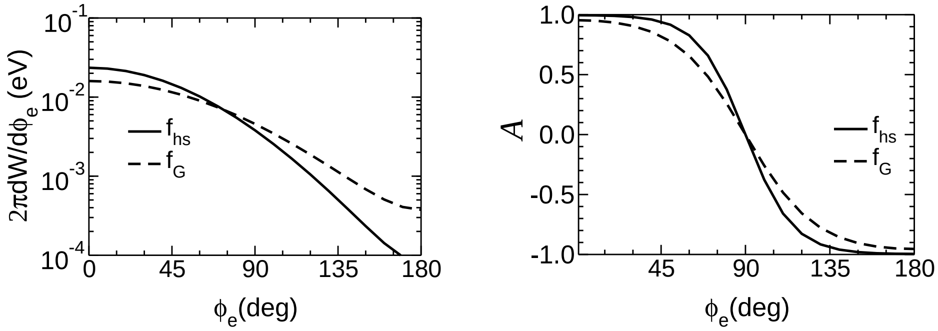

FIG. 5: Left panel: The differential production probability as a function of the azimuthal angle ϕ_e of the electron emission. Right panel: The anisotropy (26) for the hyperbolic secant (solid curves) and Gaussian (dashed curves) shapes. For $\xi^2 = 0.1$ and $\zeta = 4$.

The differential probability of the e^+e^- pair emission and the anisotropy as a function of the azimuthal angle ϕ_e are exhibited in Fig. 5. The calculations are for the fast-decreasing one-parameter envelope functions for $\Delta = 0.5\pi$, $\zeta = 4$ and $\xi^2 = 0.1$. One can see a rapidly decreasing probability with ϕ_e which leads to the strong anisotropy of electron (positron) emission.

In case of the symmetrized Fermi distribution with small b/Δ, the situation changes drastically. As $b/\Delta \to 0$ the envelope function goes to the flat-top (step-like) shape $f_{\rm Fs}(\phi) \to \theta(\Delta^2 - \phi^2)$ with $\theta(x) = 1$, 0 for $x \geq 0$ or $x < 0$, respectively, and correspondingly

$$\mathcal{Y}(l) = \frac{1}{2\pi}\int\limits_{-\Delta}^{\Delta} d\phi\, \mathrm{e}^{i\left[\tilde{l}\phi - z\sin(\phi-\phi_0)\right]} \tag{27}$$

with $\tilde{l} = l + \xi^2\zeta u$. The function $\mathcal{Y}(l)$ in the region $\zeta \leq l < l_{\rm max} \gg 1$ is alternating, rapidly oscillating with an amplitude that depends only on ξ, ζ, and u. It is not sensitive to ϕ_0. Modifications of ϕ_0 lead some phase shift of $\mathcal{Y}(l)$ in a range of integration, leaving $\langle|\mathcal{Y}(l)|^2\rangle$ to be independent of ϕ_0 Therefore, the dependence of the integral of the partial probability $w(l) \sim |\mathcal{Y}(l)|^2$ in Eq. (13) on ϕ_0 is negligible. As an example, in the left panel of Fig. 6 we present the partial probability $w(l)$ as a function of l, calculated at $\xi^2 = 0.1$, $\zeta = 4$ and $u = 1$ for the small values of b/Δ equal to 0.1 and 0.01 at $\phi_0 = 0$ and π, shown by solid and dashed curves, respectively. One can see some small modification of the frequency of oscillations at $l \sim l_{\rm min} = \zeta$ at two extreme values of ϕ_0, but the amplitudes of the oscillations

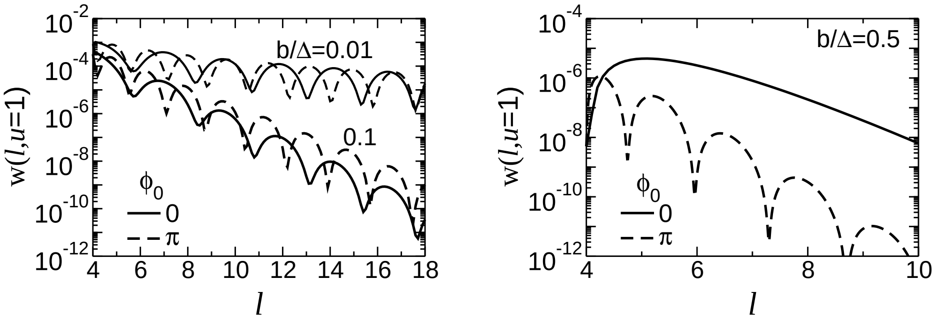

FIG. 6: The partial probability $w(l)$ defined in (13) at $\phi_0 = 0$ and π shown by solid and dashed curves, respectively, for the symmetrized Fermi envelope shape. The left panels correspond to small values of b/Δ =0.01 and 0.1, while the right panel is for $b/\Delta = 0.5$. For $\xi^2 = 0.1$ and $\zeta = 4$.

are similar. This situation is quite different from the case of the large value of $b/\Delta = 0.5$ presented in the right panel of Fig. 6. One can see a strong difference in the l-dependence of $w(l)$ for $\phi_0 = 0$ and π. In the first case, the function $w(l)$ has only one oscillation in a wide range of l and decreases smoothly with l. In the second case, the probability has a number of oscillations decreasing rapidly with increasing l. As a result, the total probability in the second case is much smaller.

This behavior can also be understood from a different point of view. The integral over l of the derivative of the partial probability $w(l)$ in Eq. (13)

$$\frac{dw(l)}{d\phi_0} \sim \frac{d}{d\phi_0} |\mathcal{Y}(l|^2 \sim |\mathcal{Y}(l \pm 1)\mathcal{Y}(l)| \tag{28}$$

is vanishing because of the alternating and oscillating nature of $\mathcal{Y}(l)$. Therefore, the probability W is independent of ϕ_0.

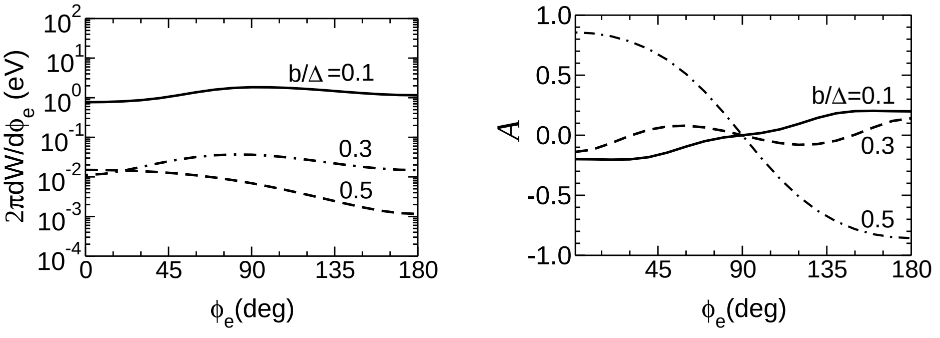

FIG. 7: The same as in Fig. 5 but for the symmetrized Fermi shape. The solid, dot-dashed and dashed curves are for $b/\Delta = 0.1$, 0.3 and 0.5, respectively. For $\xi^2 = 0.1$ and $\zeta = 4$.

In Fig. 7 we present our results for the symmetrized Fermi shape for the production probability (left panel) and for the anisotropy (right panel) for $b/\Delta = 0.1$, 0.3 and 0.5. The result for $b/\Delta = 0.5$ is similar to that shown in Fig. 5. However, for smaller values of b/Δ, the probability is a smooth function of ϕ_0 with some modest enhancement around $\pi/2$, which leads to a negligible anisotropy.

IV. SHORT PULSES

In this section we consider short pulses with the number of oscillation $N \geq 2$, however, many results are valid even for pulses with $N \sim 1$. As we have seen, the one-parameter envelope shapes lead to similar results even for ultra-short pulses, therefore, later on we will limit our consideration to two extreme envelope shapes: hyperbolic secant and symmetrized Fermi shape with $b/\Delta = 0.1$.

As mentioned above, Eqs. (13) and (14) can be used for numerical estimates of the e^+e^- production probability evaluating five dimensional integral(s) with rapidly oscillating functions. Technically, such an approach needs long calculation time which makes it difficult for applications in transport/Monte Carlo codes. However, a closer inspection of the functions $\mathcal{P}(\phi)$ and $C^{(i)}(l)$ shows that the number of integrations may be reduced and, in some cases, Eq. (14) may be expressed in an analytical form. Thus, integrating by parts the function $\mathcal{P}(\phi)$ might be rewritten in the following form

$$\mathcal{P}(\phi) \equiv \mathcal{P}_0(\phi) - \xi^2 \zeta u \int\limits_{-\infty}^{\phi} d\phi' \, f^2(\phi'), \qquad \mathcal{P}_0(\phi) = z \left(\sin(\phi - \phi_0) f(\phi) + \mathcal{O}\left(\frac{1}{\Delta}\right) \right) \tag{29}$$

with

$$\mathcal{O}\left(\frac{1}{\Delta}\right) = -\frac{1}{\Delta} \int\limits_{-\infty}^{\phi} d\phi' \, \sin(\phi' - \phi_0) f'(\phi') \; . \tag{30}$$

The contribution of this term to $\mathcal{P}(\phi)$ is sub leading for the finite pulse size $\Delta = \pi N$ with $N \geq 2$. First, because of the explicit factor $1/\Delta$, and second because the derivative $f'(\phi)$ in the integrand reaches its maximum value at the boundaries of the pulse, where this function is suppressed. For an illustration, in Fig. 8 we present results of a numerical analysis of $\mathcal{P}_0(\phi)$ with the hyperbolic secant envelope function. The solid and dashed curves exhibit calculations with and without the term (30), respectively for $\phi_0 = 0$ and π. The left and right panels correspond to $\Delta = \pi N$ with $N = 2$ and 5, respectively. The term $(|\mathcal{O}(1/\Delta)|)$ is shown by dot-dashed curves. One can see, in fact, that this term is rather small and may be omitted. For the flat-top envelopes this approximation is even much better.

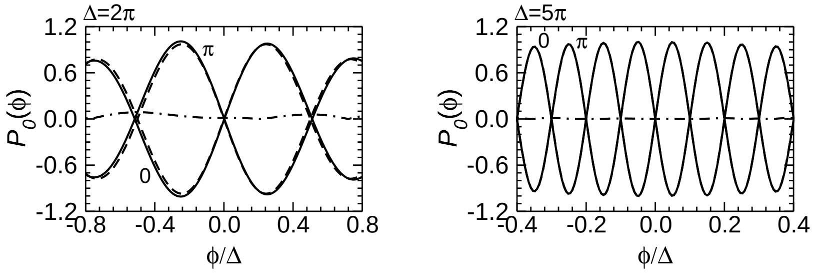

FIG. 8: The function $\mathcal{P}_0(\phi)$ defined in (29) with (solid curves) and without (dashed curves) the term (30) for $\Delta = \pi N$ with $N = 2$ and 5, shown in left and right panels, respectively. The term (30) is shown separately by dot-dashed curves.

Using this approximation one can express the basic functions $C^{(i)}(l)$ defined in Eqs. (6) and (11) through the new functions Y_l and X_l, which may be considered as an analog of the Bessel functions in IPA,

$$\begin{aligned}
Y_l(z) &= \frac{1}{2\pi}\int\limits_{-\infty}^{\infty} d\psi\, \tilde{f}(\psi+\phi_0)\, \mathrm{e}^{il\psi - iz\sin\psi} \ , \\
X_l(z) &= \frac{1}{2\pi}\int\limits_{-\infty}^{\infty} d\psi\, \tilde{f}^2(\psi+\phi_0)\, \mathrm{e}^{il\psi - iz\sin\psi} \ , \\
\tilde{f}(\phi) &= f(\phi)\, \exp[i\xi^2\zeta\, u\, r(\phi)] \ , \qquad \tilde{f}^2(\phi) = f^2(\phi)\, \exp[i\xi^2\zeta\, u\, r(\phi)] \ , \\
r(\phi) &= \int\limits_{-\infty}^{\phi} d\phi'\, f^2(\phi') \ ,
\end{aligned} \tag{31}$$

where the function $r(\phi)$ is a smooth function of ϕ. For the hyperbolic secant we have $r(\phi) = \Delta\tanh(\phi/\Delta)$, where we skip the constant term which does not contribute; for the flat-top envelope, $r(\phi) \sim \phi\,\theta(\Delta^2 - \phi^2)$. The new representation of the basic functions $C^{(i)}(l)$ reads

$$\begin{aligned}
C^{(1)}(l) &= X_l(z)\, \mathrm{e}^{i(l)\phi_0} \ , \\
C^{(2)}(l) &= \frac{1}{2}\left(Y_{l+1}\mathrm{e}^{i(l+1)\phi_0} + Y_{l-1}\mathrm{e}^{i(l-1)\phi_0}\right) \ , \\
C^{(3)}(l) &= \frac{1}{2i}\left(Y_{l+1}\mathrm{e}^{i(l+1)\phi_0} - Y_{l-1}\mathrm{e}^{i(l-1)\phi_0}\right) \ ,
\end{aligned}$$

$$C^{(0)}(l) \ = \ \widetilde{Y}_l(z)\mathrm{e}^{i(l)\phi_0}, \qquad \widetilde{Y}_l(z) = \frac{z}{2l}\left(Y_{l+1}(z) + Y_{l-1}(z)\right) - \xi^2 \frac{u}{u_l} X_l(z) \ . \tag{32}$$

It allows to express $w(l)$ in Eq. (14) in the form

$$w(l) = 2\widetilde{Y}_l^2(z) + \xi^2(2u-1)\left(Y_{l-1}^2(z) + Y_{l+1}^2(z) - 2\widetilde{Y}_l(z)X_l^*(z)\right) \ , \tag{33}$$

which resembles the expression for the probability in case of IPA (cf. Eq. (A1)). Now we are going to discuss separately the weak-, intermediate- and strong-field regimes.

A. Production probability at small field intensities ($\xi^2 \ll 1$)

In case of small values of ξ^2, $\xi^2 \ll 1$, implying $z < 1$, we decompose $l = n + \epsilon$, where n is the integer part of l, yielding

$$\begin{aligned} Y_l \ &\simeq \ \frac{1}{2\pi}\int\limits_{-\infty}^{\infty} d\psi \, \mathrm{e}^{il\psi - iz\sin\psi} f(\psi+\phi_0) \\ &= \ \frac{1}{2\pi}\int\limits_{-\infty}^{\infty} d\psi \sum_{m=0}^{\infty} \frac{(iz)^m}{m!} \sin^m\psi \, \mathrm{e}^{i(n+\epsilon)\psi} f^{m+1}(\psi+\phi_0) \ . \end{aligned} \tag{34}$$

Similarly, for the function $X_l(z)$ the substitution $f^{m+1} \to f^{m+2}$ applies. The dominant contribution to the integral with rapidly oscillating integrand comes from the term with $m = n$, which result in

$$Y_{n+\epsilon} \simeq \frac{z^n}{2^n n!}\,\mathrm{e}^{-i\epsilon\phi_0} F^{(n+1)}(\epsilon) \ , \qquad X_{n+\epsilon} \simeq \frac{z^n}{2^n n!}\,\mathrm{e}^{-i\epsilon\phi_0} F^{(n+2)}(\epsilon) \ , \tag{35}$$

where the function $F^{(n)}(\epsilon)$ is the Fourier transform of the function $f^n(\psi)$.

As an example, let us analyze the e^+e^- production near the threshold, i.e. $\zeta \sim 1$. In this case, the contribution with $n = 1$ is dominant and, therefore, the functions $Y_{0+\epsilon}$ are crucial, including the first term in (33). The functions $X_{0+\epsilon}$ are not important because they are multiplied by the small ξ^2 and may be omitted. Negative $\epsilon = \zeta - 1$ and positive ϵ correspond to the above- and sub-threshold pair production, respectively. The function $Y_{0+\epsilon}$ reads $Y_{0+\epsilon} = F^{(1)}(\epsilon)\exp[-i\phi_0\epsilon]$ with corresponding Fourier transform $F^{(1)}(\epsilon)$ presented in Eq. (22). Note that the ϕ_0-dependence of the production probability disappears in this case because the latter one is determined by the quadratic terms of the Y-function.

Consider first the pair production above the threshold. Keeping the terms with leading power of ξ^2 one can express the production probability as

$$\frac{dW}{du} = \frac{\alpha M_e \zeta^{1/2}}{4N_0} \left[\frac{u}{u_1}\left(1 - \frac{u}{u_1}\right) + u - \frac{1}{2}\right] \frac{\xi^2}{u^{3/2}\sqrt{(u-1)}} I_0 \ , \tag{36}$$

where, taking into account that, at finite values of Δ, Fourier transforms for all considered envelopes decrease rapidly with increasing ϵ one can get

$$I_0 \simeq \int\limits_{1-\zeta}^{1/2} d\epsilon\, F^{(1)2}(\epsilon) \simeq \int\limits_{-\infty}^{\infty} d\epsilon\, F^{(1)2}(\epsilon) = \frac{1}{2\pi} \int\limits_{-\infty}^{\infty} d\phi\, f^2(\phi) \simeq N_0 \ . \tag{37}$$

Combining these two equations one recovers exactly the IPA result [6]. Thus, we can conclude that for small field intensities for a finite pulse duration the probabilities of e^+e^- pair emission above threshold with $\zeta < 1$ results in a coincidence of IPA and FPA, independently of the shape of the envelope function. For an illustration, in Fig. 9 we show the partial probability $w(l)$, calculated at $u = 1$ for the above-threshold region with $\xi^2 = 10^{-2}$ and $\zeta = 0.5$ in a finite region of l for the envelope size $\Delta = \pi N$ with $N = 2$ and 10, respectively. For the envelope with a hyperbolic secant shape (left panel) one can see smooth curves with maxima at integer values of l. The widths of bumps decrease with increasing N. However, the integral of $w(l)$ over l in the neighborhood of the first maximum is independent of N and coincides with the contribution of the first harmonic in IPA which leads to an equality of IPA and FPA results. For the symmetrized Fermi shape (right panel) the situation is

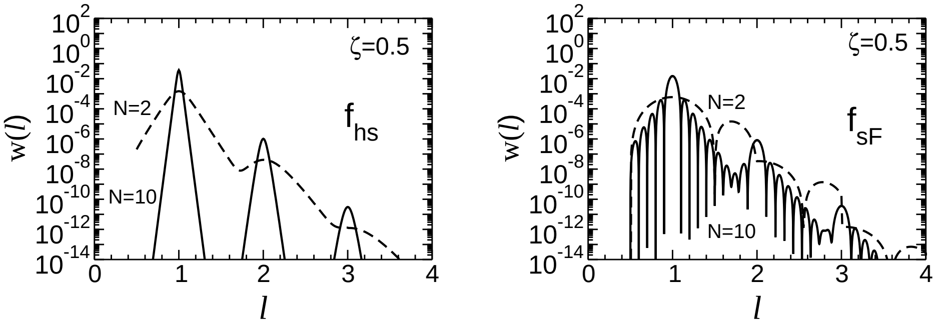

FIG. 9: The partial probability $w(l)$ defined in (33) as a function of l at $u = 1$. The solid and dashed curves correspond to the beam size $\Delta = \pi N$ with $N = 2$ and 10, respectively. Left and right panels exhibit results for the envelopes with hyperbolic secant and symmetrized Fermi shapes, respectively. For $\xi = 10^{-4}$ and $\zeta = 0.5$

different in some sense. The corresponding Fourier transforms $F_{sF}^{(n)}(l)$ in (35) oscillate with l. For example, the function $F_{sF}^{(1)}$ goes to zero at a multiple of $1/N$. This results in an oscillating structure of $w(l)$. However, the exponential decrease of $w(l)$ with increasing of the integer values of l is the same.

The situation changes when we are slightly below threshold, i.e. $\zeta > 1$. In this case, the function $Y_{0+\epsilon}$ dominates again and the result for FPA is the same as in (36) but with the substitution $I_0 \to I_1$, with $I_1 \simeq \int\limits_{\zeta-1}^{1} d\epsilon\, F^{(1)2}(\epsilon)$. In case of smooth envelope shape (e.g. hyperbolic secant) the dominating contribution to this integral comes from the lower limit and, therefore, $I_1 \sim \left(F_{\rm hs}^{(1)}(\zeta-1)\right)^2$. As a result, the production probability strongly depends on the duration Δ of the pulse.

In case of a flat-top envelope, we have a similar effect, because $F_{sF}^{(1)}(l)$ in general decreases exponentially as $\exp(-\pi b l)$, where b increases with increasing N at fixed b/Δ.

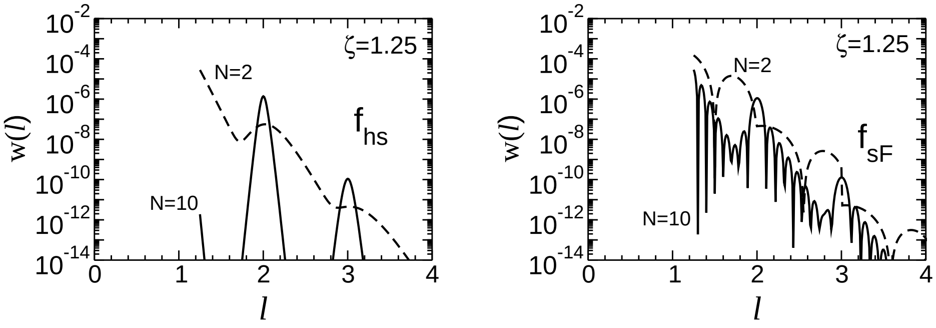

FIG. 10: The same as in Fig. 9 but for the sub-threshold region at $\zeta = 1.25$.

In Fig. 10 we show the partial probability $w(l)$ in the sub-threshold region, i.e. $\zeta = 1.25$. One can see that for the hyperbolic secant envelope (left panel) the difference of $w(l)$ at $l \simeq \zeta$ for $N = 2$ and $N = 10$ is more than several orders of magnitude, which will be reflected in the total probability. In the case of the symmetrized Fermi envelope shape, one also can see a significant enhancement of $w(l)$ for $N = 2$ compared to $N = 10$. But now, the difference between FPA and IPA is larger compared to the case of the hyperbolic secant shape.

The total probability W of e^+e^- emission as a function of the sub-threshold parameter ζ in the vicinity $\zeta \sim 1$ is presented in Fig. 11. The left and right panels correspond the hyperbolic secant and symmetrized Fermi envelope shapes, respectively. Calculations are performed for short pulses with $N = 2$, 5 and 10 oscillations in the pulse at $\xi^2 = 10^{-3}$. For comparison, we present also the IPA results. In the above-threshold region, results of IPA and FPA are

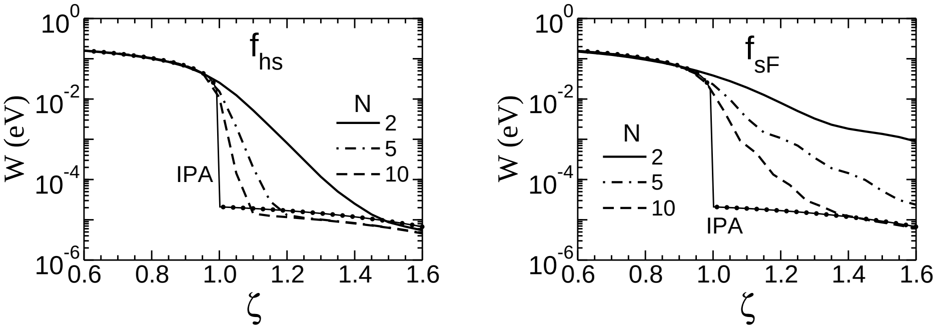

FIG. 11: The total probability W of the e^+e^- pair production as a function of ζ for short pulses with $\Delta = \pi N$ for $N = 2$, 5 and 10 as indicated in the legend. The thin solid curves marked by dots depict the IPA result. Left and right panels correspond to the hyperbolic secant and symmetrized Fermi envelope shapes, respectively.

equal to each other according to Eqs. (36) and (37). However, in the sub-threshold region, where ζ is close to unity, the probability of FPA considerably (by more than two orders of magnitude) exceeds the corresponding IPA result. In case of the hyperbolic secant envelope function the probability increases with decreasing pulse duration. The results of FPA and IPA become comparable at $N \geq 10$. Qualitatively, this behavior is true for the case of the symmetrized Fermi distribution. However, in this case, the enhancement of the probability in FPA is much greater. This is due to the fact that the envelope of the maxima in the partial probability $w(l)$ (cf. Fig. 10) decreases with increasing l in different ways for different envelope shapes. In case of the hyperbolic secant it decreases as $\exp(-\pi\Delta l)$, whereas in case of symmetrized Fermi shape it decreases as $\exp(-2\pi bl)$. For the latter one, at $b/\Delta = 0.1$ the slope is much smaller. Such a strong gain of e^+e^- emission is expected for other values of ζ when ζ exceeds an integer number. This effect is illustrated in Fig. 12, where the total e^+e^- production probability W is presented in a wide region of ζ at $\xi = 0.01$. For convenience, we show also results for two different pulse shapes simultaneously. For two oscillations in a pulse (left panel $N = 2$), for the hyperbolic secant shape one can see a regular enhancement of the probability W when ζ exceeds the corresponding integer value. As a result, $W(\zeta)$ in FPA is a smooth function, while a step-like dependence of the probability appears in IPA. For the flat-top, symmetrized Fermi distribution at $\zeta > 1$, the probability is significantly larger than for hyperbolic secant pulse shape and displays a step-like behavior. The latter one, however, is related mainly to the oscillating nature of the corresponding Fourier transform

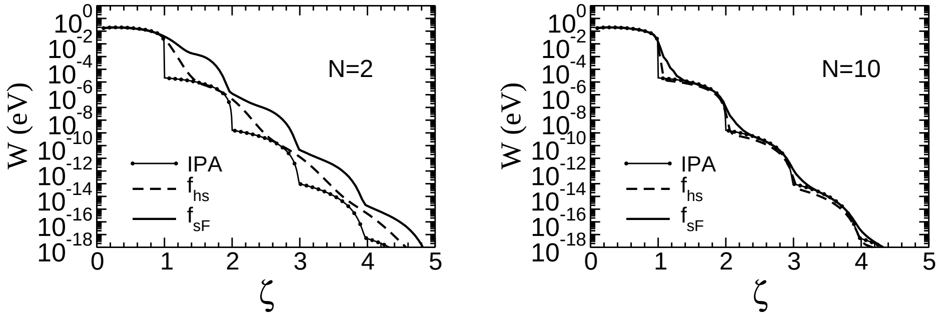

FIG. 12: The total probability W of the e^+e^- pair production as a function of ζ for one- and two-parameter envelope shapes (dashed and solid curves are for hyperbolic secant and symmetrized Fermi shapes, respectively). The thin solid curves marked by dots depict the IPA result. Left and right panels correspond to the number of oscillation in a pulse $N = 2$ and 10, respectively.

in (35).

At large values of N (right panel, $N = 10$) results of FPA and IPA become close to each other, especially for the one-parameter envelope shapes. For this case, at least for $\xi = 0.01$, $N \simeq 10$ can be considered to be near infinite, when considering the overall ζ dependence. For the flat-top shape with small b/Δ the probability in FPA is higher than the result of IPA near integer values of ζ.

To summaries this part we have to note that temporal beam shape effects for short pulses are strong and even dominant at small field intensities in the parameter region where the variable z is small, $z \ll 1$. At finite z, the non-linear dynamics of $e^\pm$ in the strong pulse becomes essential.

B. Production probability at intermediate field intensities ($\xi^2 \sim 1$)

At finite values of z, $z \gtrapprox 1$, the probability of e^+e^- emission needs to be calculated numerically using Eqs. (13), (31) and (33). In Fig. 13, we present the total probability W as a function of ζ at fixed $\xi^2 = 1$ (left panel) and as a function of ξ^2 at fixed $\zeta = 4$ (right panel). The calculations are performed for the hyperbolic secant and symmetrized Fermi pulse envelope shapes, shown by the dashed and solid curves, respectively. The duration of the pulse is $\Delta = \pi N$ with $N = 2$. For comparison, we also present IPA results by the thin solid curves marked by dots. At finite ξ^2, the probability decreases monotonically with increasing ζ (left panel), contrary to the step-like decrease typical for the small $\xi^2 \ll 1$ (cf.

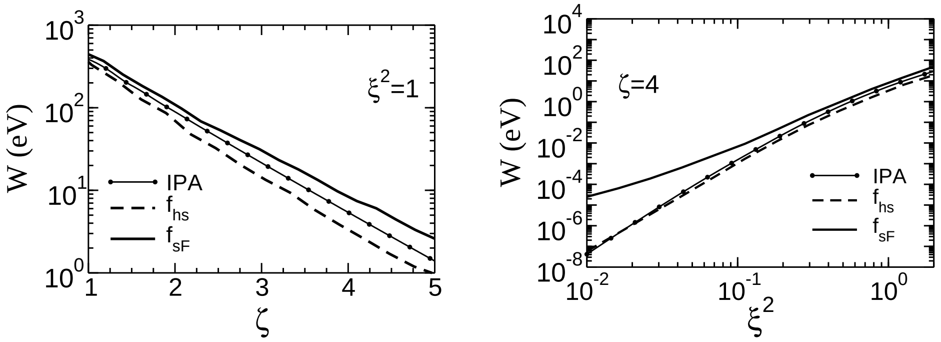

FIG. 13: The total probability of e^+e^--pair production for two envelope shapes (dashed and solid curves are for hyperbolic secant and symmetrized Fermi shapes, respectively). The thin solid curves marked by dots are the result of IPA. Left panel: The total probability as a function of ζ at $\xi^2 = 1$. Right panel: The total probability as a function of ξ^2 at $\zeta = 4$.

Fig. 12). The probability for the flat-top pulse shape slightly exceeds the probability for the hyperbolic secant and the IPA result.

Concerning the ξ^2 dependence (right panel), one can see a significant enhancement of the total probability W at small values of ξ^2 for the flat-top pulse shape compared to the case of hyperbolic secant and the IPA result. The latter two results are practically identical to each other. At $\xi^2 > 1$, the production probability does not sensitively depend on the pulse shape, and FPA and IPA results are close to each other. This means that at large field intensity the dynamical aspects of the pair production gain a dominant role in comparison with the pulse shape and size effects.

Finally, we note that, at finite ξ^2, the dependence of the probability on the azimuthal angle ϕ_e disappears and the distribution in the $x - y$ plane becomes isotropic. As an

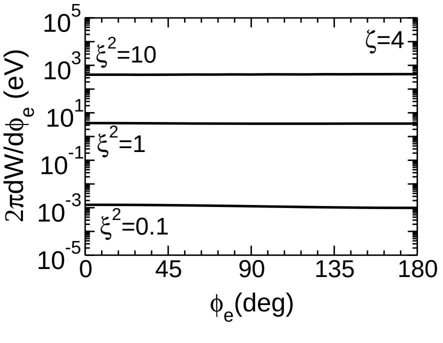

FIG. 14: The differential probability of e^+e^--pair production as a function of $\phi_e = \phi_0$ at $\zeta = 4$ and $N = 2$.

example, in Fig. 14 we present results of calculations of the differential probability of e^+e^--pair production as a function of $\phi_e = \phi_0$ at $\zeta = 4$ for the hyperbolic secant pulse shape with $N = 2$ at $\xi^2 = 0.1$, 1 and 10. The results reflect the isotropy of the e^+e^- emission and expose the ξ^2 dependence.

C. Production probability at large field intensity ($\xi^2 \gg 1$)

At large values of ξ^2, $\xi^2 \gg 1$, the basic functions Y_l and X_l in Eq. (31) can be expressed in the form of (18):

$$Y_l = \int\limits_{-\infty}^{\infty} dq\, F^{(1)}(q)\, G(l-q)\ , \qquad X_l = \int\limits_{-\infty}^{\infty} dq\, F^{(2)}(q)\, G(l-q)\ , \tag{38}$$

where $F^{(1)}(q)$ and $F^{(2)}(q)$ are Fourier transforms of the functions $f(\phi)$ and $f^2(\phi)$, respectively, and $G(l)$ may be written as

$$G(l) = \frac{1}{2\pi}\int\limits_{-\infty}^{\infty} d\phi\, \mathrm{e}^{i\left(l\phi - z\sin\phi + \xi^2\zeta u\phi\right)}\ . \tag{39}$$

In deriving this equation we have considered the following facts: (i) at large ξ^2 the probability is isotropic, therefore we put $\phi_0 = 0$, (ii) the dominant contribution to the rapidly oscillating exponent comes from the region $\phi \simeq 0$, where the difference of two large values $l\phi$ and $z\sin\phi$ is minimal, and therefore, one can decompose the last term in the function $\mathcal{P}(\phi)$ in (29) around $\phi = 0$, and (iii) replace in exponent $f(\phi)$ by $f(0) = 1$.

Equation (39) represent an asymptotic form of the Bessel functions [34] $J_{\tilde{l}}(z)$ with $\tilde{l} = l + \xi^2\zeta u$ at $\tilde{l} \gg 1$, $z \gg 1$, and therefore the following identities are valid

$$G(l-1) - G(l+1) = 2G'_z(l), \qquad G(l-1) + G(l+1) = 2\frac{\tilde{l}}{z}G(l)\ , \tag{40}$$

which allow to express the partial probability $w(l)$ in (33) as a sum of the diagonal (relative to l) terms: Y_l^2, $Y_l X_l$, X_l^2 and $Y_l^{'2}$. The integral over l from the diagonal term can be expressed as

$$I_{YY} = \int\limits_{\zeta}^{\infty} dl\, Y_l^2 = \int dq\, dq' F^{(1)}(q)\, F^{(1)}(q') \int\limits_{\zeta}^{\infty} dl G(l-q) G(l-q')\ . \tag{41}$$

Taking into account that for the rapidly oscillating G functions $G(l-q)G(l-q') \simeq \delta(q-q')G^2(l-q)$ and $\langle q\rangle \ll \langle l\rangle \ \sim \xi^2$ one gets

$$I_{YY} = \frac{1}{2\pi}\int\limits_{-\infty}^{\infty} d\phi f^2(\phi) \int\limits_{\zeta}^{\infty} dl G^2(l) = N_{YY}\int\limits_{\zeta}^{\infty} dl G^2(l)\ . \tag{42}$$

Similar expressions are valid for the other diagonal terms with own normalization factors. For the X_l^2 term it is $N_{XX} = \frac{1}{2\pi}\int\limits_{-\infty}^{\infty} d\phi f^4(\phi)$, and for $Y_l X_l$, $N_{YX} = \frac{1}{2\pi}\int\limits_{-\infty}^{\infty} d\phi f^3(\phi)$. At large ξ^2, the probability does not depend on the envelope shape, because only the central part of the envelope is important. Therefore, for simplicity, we choose the flat-top shape with $N_{YY} = N_{YX} = N_{XX} = N_0 = \Delta/\pi$ which is valid for any smooth (at $\phi \simeq 0$) envelopes.

Making a change of the variable $l \to \tilde{l} = l + \xi^2\zeta u$ the variable z takes the following form

$$z^2 = 4\xi^2\zeta^2\left(uu_l - u^2\right) = \frac{4\xi^2 l_0^2}{1+\xi^2}\left(uu_{\tilde{l}} - u^2\right) \tag{43}$$

with $l_0 = \zeta(1+\xi^2)$ and $u_{\tilde{l}} \equiv \tilde{l}/l_0$, that is exactly the same as the variable z in IPA with the substitution $l \to \tilde{l}$. All these transformations allow to express the total probability in a form similar to the probability in IPA for large values of ξ^2 and a large number of partial harmonics n, replacing sum of n by an integral over n [6]

$$W = \frac{1}{2}\alpha M_e \zeta^{1/2}\int\limits_{l_0}^{\infty} d\tilde{l}\int\limits_{1}^{u_{\tilde{l}}} \frac{du}{u^{3/2}\sqrt{u-1}}\left\{J_{\tilde{l}}^2(z) + \xi^2(2u-1)\left[(\frac{\tilde{l}^2}{z^2}-1)J_{\tilde{l}}^2(z) + J'^2_{\tilde{l}}(z)\right]\right\}\ . \tag{44}$$

Utilizing Watson's representation [34] for the Bessel functions at $\tilde{l}$, $z \gg 1$ and $\tilde{l} > z$, $J_{\tilde{l}}(z) = (2\pi\tilde{l}\tanh\alpha)^{-1/2}\exp[-\tilde{l}(\alpha - \tanh\alpha)]$ with $\cosh\alpha = \tilde{l}/z$, and employing a saddle point approximation in the integration in (44) we find the total probability of e^+e^- production as (for details see Appendix A)

$$W = \frac{3}{8}\sqrt{\frac{3}{2}}\frac{\alpha M_e \xi}{\zeta^{1/2}}\, d\, \exp\left[-\frac{4\zeta}{3\xi}(1-\frac{1}{15\xi^2})\right],\ d = 1 + \frac{\xi}{6\zeta}\left(1+\frac{\xi}{8\zeta}\right)\ . \tag{45}$$

This expression coincides with the production probability in IPA which is the consequence of the fact that, at $\xi^2 \gg 1$ in a short pulse, only the central part of the envelope at $\phi \simeq 0$ is important. Approximating $d = 1 + \mathcal{O}(\xi/\zeta)$, the leading order term recovers the Ritus result [6].

For completeness, in Fig. 15 (left panel) we present FPA results for not too large values of ξ^2 calculated for the hyperbolic secant envelope shape with $N = 2$ (curves are marked

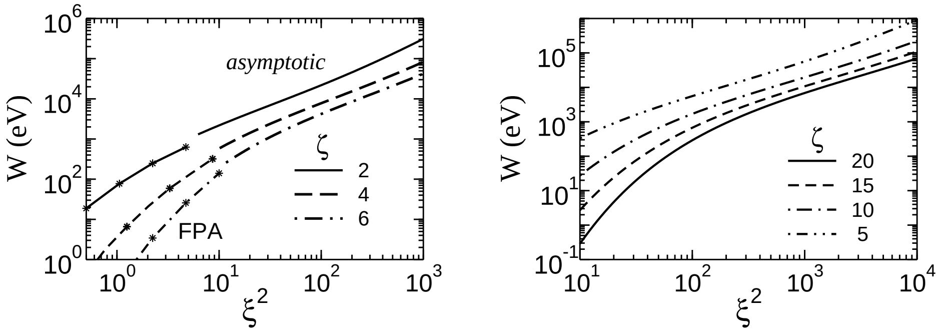

FIG. 15: The total probability W of the e^+e^- pair production as a function of ξ^2 for various values of ζ. Left panel: Results of FPA for not too large values of ξ^2 (curves marked by "stars" in "FPA" sections) and the asymptotic probability (45) for large values of ξ^2 (sections labeled by "asymptotic") at $\zeta = 2$, 4 and 6. Right panel: The asymptotic probability (45) for various values of ζ as indicated in the legend.

by "stars") and the asymptotic probability calculated by Eq. (45) at $\zeta = 2$, 4 and 6. The transition region between the two regimes is in the neighborhood of $\xi^2 \simeq 10$. In the right panel, we show the production probability at asymptotically large values of ξ^2 for $5 \leq \zeta \leq 20$. The exponential factor in (45) is most important at the relatively low values of $\xi^2 \sim 10$ (large ζ/ξ). At extremely large values of ξ^2 (small ζ/ξ) the per-exponential factor is dominant.

V. SUMMARY

In summary we have considered different aspects of e^+e^- pair production in a strong electromagnetic field of a finite (laser) pulse, thus generalizing the Breit-Wheeler process to non-linear (i.e. multi-photon) effects. The pair production in the sub-threshold region with $\zeta > 1$ is currently a subject of great interest. We have shown that the production probability is determined by a non-trivial interplay of two dynamic effects. The first one is related to the shape and duration of the pulse. The second one is the non-linear dynamics of charged particles in the strong electromagnetic field itself, independently of the pulse geometry.

These two effects play quite different roles in two limiting cases.

(i) The pulse shape effects are manifest clearly at small values of product the $\xi\zeta$, where ξ characterizes the laser intensity and ζ refers to the threshold kinematics. The rapid variation of the e.m. field in a very short pulse amplifies the multi-photon events, and moreover, the probability of multi-photon events in FPA can exceed the IPA prediction by orders of magnitude. Thus, for example in case of an ultra-short (sub cycle) pulse with the number of oscillations N in the pulse less than one, the production probability as a function of ζ is almost completely determined by the square of the Fourier transform of the pulse envelope function. High-l components, where l is the Fourier conjugate to the invariant phase variable ϕ, lead to the enhancement of the production probability. Among the considered envelope shapes, the flat-top shape with small b/Δ is most promising to obtain the highest probability. We also find that the different envelope shapes lead to anisotropies of the electron (positron) emission which can be studied experimentally. For short pulses with $N < 10$, the effects of the pulse shape are also important and the final yield differs significantly from the IPA prediction. This difference depends on the envelope shapes and the pulse duration.

(ii) Contrary to that, the non-linear multi-photon dynamics of $e^{\pm}$ in the strong electromagnetic field plays the determining role at large field intensities, $\xi^2 \gg 1$. Here, the effects of the pulse shape and duration disappear since the dominant contribution comes from the central part of the envelope function. As a result, the probabilities in FPA and IPA coincide.

In the transition region of intermediate intensities $\xi^2 \sim 1$, the probability is determined by the interplay of the both effects, and they must be taken into account simultaneously by a direct numerical evaluation of the multi-dimensional integrals with rapidly oscillating integrands.

Finally, we emphasize that the elaborated methods can be applied easily in transport approaches aimed at studying e^+e^- pair production in the interaction of electrons/positrons and/or photons with a finite electromagnetic (laser) pulse.

Acknowledgments

The authors acknowledge fruitful discussions with H. Ruhr, D. Seipt, and T. Nousch. The support by R. Sauerbrey and T. E. Cowan is gratefully acknowledged.

Appendix A: Production probability at large values of ξ

The total probability W in the limit of large ξ and and small ξ/ζ, was evaluated by Narozhny, Nikishov and Ritus [6]. for completeness and easy reference, we recall here some details of evaluation making expansion for an arbitrary ξ/ζ.

In IPA, the total probability is represented as an infinite sum of partial harmonics [6]

$$W \;=\; \frac{1}{4}\alpha M_e \zeta \sum_{n=n_0}^{\infty} \int\limits_{1}^{u_n} \frac{du}{u^{3/2}\sqrt{u-1}} \left\{ 2J_n^2(z) + \xi^2(2u-1)\left(J_{n+1}^2(z) + J_{n-1}^2(z) - 2J_n^2(z)\right)\right\} , \tag{A1}$$

where $n_0 \equiv n_{\min} = \zeta(1+\xi^2)$, $u_n = n/n_0$, and $J_n(z)$ is the Bessel function of the first kind (cylindrical harmonics). Using the identities

$$2\,\frac{n}{z}\,J_n(z) = J_{n-1}(z) + J_{n+1}(z), \;\; 2\,J'_n(z) = J_{n-1}(z) - J_{n+1}(z)\ , \tag{A2}$$

the total probability takes the following form

$$W = \frac{1}{2}\alpha M_e \zeta^{1/2} \sum_{n_0}^{\infty} \int\limits_{1}^{u_n} \frac{du}{u^{3/2}\sqrt{u-1}} \left(J_n^2(z) + \xi^2(2u-1)\left((\frac{n^2}{z^2} - 1)J_n^2(z) + J'^2_n(z) \right)\right) . \tag{A3}$$

At large $\xi \gg 1$, $\zeta \gg 1$, n, $z \gg 1$ and $n > z$ one can replace the sum over integer n by an integral over dn, replacing, for convenience, integer n to continues l with $l_{\min} \equiv l_0 = \zeta(1+\xi^2)$. Using Watson's asymptotic expression for the Bessel functions one finds

$$J_l\left(\frac{l}{\cosh\alpha}\right) = \frac{1}{\sqrt{2\pi l \tanh\alpha}} e^{-l(\alpha - \tanh\alpha)} + \mathcal{O}\left(\frac{1}{\xi}\right) \tag{A4}$$

with $\cosh\alpha = l/z$. If l is large the first term represents a good approximation irrespectively whether ξ/ζ is small or large [34]. The corresponding derivative reads

$$J'_l(z) \simeq \sinh\alpha\, J_l(z)\, \left(1 + \frac{1}{2l\sinh^2\alpha\tanh\alpha}\right)\ . \tag{A5}$$

Consider first the case of small $\xi/\zeta \ll 1$, when the second term in (A5) can be neglected. Then, the total probability becomes

$$W = \frac{e^2 M_e \zeta^{1/2}}{8\pi^2} \int\limits_{l_0}^{\infty} dl \int\limits_{1}^{u_l} \frac{du}{u^{3/2}\sqrt{u-1}} \frac{1 + 2\xi^2(2u-1)\sinh^2\alpha}{l\,\tanh\alpha} \exp[f(u,l)]\ , \tag{A6}$$

where $u_l = l/l_0$ and $\hat{f}(u,l) = -2l(\alpha - \tanh(\alpha))$ with

$$\tanh^2(\alpha) = \frac{1 + \xi^2\left(1 - \frac{2u}{u_l}\right)^2}{1+\xi^2}\ . \tag{A7}$$

To avoid a notational confusion with respect to the standard variable α, we replace below the fine structure constant by $e^2/4\pi$.

The two-dimensional integral is evaluated using the saddle point approximation since the function $\hat{f}(u,l)$ has a sharp minimum at the point $u = \bar{u}$ defined by the equation $\hat{f}'_u(u=\bar{u}) = 0$. That allows (i) to expand it to a Taylor series

$$f(u,l) \simeq \hat{f}(\bar{u},l) + \frac{1}{2}\hat{f}_u{}''(\bar{u},l)(u-\bar{u})^2 \ , \tag{A8}$$

and (ii) to take the rest (smooth) part of the integrand in Eq. (A6) at the point $u = \bar{u}$ yielding

$$W = \frac{e^2 M_e \zeta^{1/2}}{16\pi^2} \int\limits_{l_0}^{\infty} dl\, \mathcal{A}_0(\bar{u},l) \mathrm{e}^{\hat{f}(\bar{u},l)} \int\limits_{1}^{u_l} \frac{du}{\sqrt{u-1}} \mathrm{e}^{\frac{1}{2}\hat{f}''(\bar{u},l)(u-\bar{u})^2} \ , \tag{A9}$$

with

$$\mathcal{A}_0(u,l) = \frac{1 + 2\xi^2(2u-1)\sinh^2\alpha}{u^{3/2} l \tanh\alpha} \ . \tag{A10}$$

The explicit expression

$$\hat{f}'_u(u,l) = \frac{4l_0 \sinh^2\alpha}{\tanh\alpha} \frac{\xi^2}{1+\xi^2} \left(1 - \frac{2u}{u_l}\right) \tag{A11}$$

leads to the solution

$$\bar{u} = \frac{u_l}{2} = \frac{l}{2l_0} \ , \tag{A12}$$

which results in the following equalities

$$\begin{aligned} &\tanh\bar{\alpha} \equiv \tanh\alpha(\bar{u}) = \frac{2}{\sqrt{1+\xi^2}}, \ \sinh\bar{\alpha} = \frac{1}{\xi}, \ \hat{f}''{}_u(\bar{u},l) = -\frac{8l_0^2}{l\sqrt{1+\xi^2}} \\ &\mathcal{A}_0 = \frac{1+2(2\bar{u}-1)}{\bar{u}^{3/2} l}\sqrt{1+\xi^2}, \ \hat{f}(\bar{u},l) = -2l(\bar{\alpha} - \tanh\bar{\alpha}) \ . \end{aligned} \tag{A13}$$

Using the substitutions $u = t+1$, $a = 2(\bar{\alpha} - \tanh\bar{\alpha})$, and $A = -\frac{1}{2}\hat{f}''(\bar{u},l)$ one can rewrite Eq. (A9) as

$$W = \frac{e^2 M_e \zeta^{1/2}}{16\pi^2} \int\limits_{l_0}^{\infty} dl\, \mathcal{A}_0(\bar{u},l) \mathrm{e}^{-al - A(1-\bar{u})^2} \int\limits_{0}^{\infty} dt\, t^{\nu-1} \mathrm{e}^{-\beta t^2 - \gamma t} \ , \tag{A14}$$

with $\nu = 1/2$, $\beta = A$, and $\gamma = 2A(1-\bar{u})$. The integral over dt is expressed via the parabolic cylinder function $D_{-\nu}$

$$\int\limits_{0}^{\infty} dt\, t^{\nu-1} \mathrm{e}^{-\beta t^2 - \gamma t} = \left(\frac{1}{2\beta}\right)^{\nu/2} \Gamma(\nu) \exp[\frac{\gamma^2}{8\beta}] \ D_{-\nu}\left(\frac{\gamma}{\sqrt{2\beta}}\right) \ , \tag{A15}$$

which results in

$$W = \frac{e^2 M_e \zeta^{1/2}}{16\pi^{3/2}} \int\limits_{l_0}^{\infty} dl \, \left(\frac{1}{2A}\right)^{\frac{1}{4}} \mathcal{A}_0(\bar{u}, l) \mathrm{e}^{-al-\frac{A}{2}(1-\bar{u})^2} D_{-\frac{1}{2}}(y) \tag{A16}$$

with $y = \sqrt{2A}(1-\bar{u})$. The main contribution to this integral comes from the region $\bar{u} \sim 1$ ($l \sim \bar{l} = 2l_0$) and, therefore, one can use the substitution

$$\int\limits_{l_0}^{\infty} dl = -\frac{2l_0}{\sqrt{2A}} \int\limits_{\sqrt{A/2}}^{-\infty} dy \approx \frac{2l_0}{\sqrt{2A}} \int\limits_{-\infty}^{\infty} dy \ , \tag{A17}$$

which results in

$$W = \frac{e^2 M_e \zeta^{1/2}}{16\pi^{3/2}} \left(\frac{1}{2A}\right)^{\frac{1}{4}} \frac{2l_0}{\sqrt{2A}} \mathcal{A}_0(\bar{u}, \bar{l}) \mathrm{e}^{-2l_0 a} \int\limits_{-\infty}^{\infty} dy \, \mathrm{e}^{Zy-y^2/4} D_{-\frac{1}{2}}(y) \tag{A18}$$

with $Z = 2l_0 a/\sqrt{2A}$. Using the identity

$$\int\limits_{-\infty}^{\infty} dy \, \mathrm{e}^{Zy-y^2/4} D_{-\frac{1}{2}}(y) = \sqrt{\frac{2\pi}{Z}} \, \mathrm{e}^{Z^2/2} \ , \tag{A19}$$

one can rewrite the production probability as

$$W = \frac{e^2 M_e \zeta^{1/2}}{16\pi} \sqrt{\frac{2l_0}{aA}} \, \mathcal{A}_0(\bar{u}, \bar{l}) \exp[-2l_0 a + \frac{l_0^2 a^2}{A}] \ . \tag{A20}$$

In order to reproduce the Ritus result [6] in terms of the kinematic factor ζ and the field intensity ξ one has to use the identity $l_0 = \zeta(1+\xi^2)$ and to represent $a(\bar{\alpha})$ as a series for small values $1/\xi$ utilizing the expansions

$$\bar{\alpha} = \mathrm{arsinh}\frac{1}{\xi} \simeq \frac{1}{\xi} - \frac{1}{6\xi^3} + \frac{3}{40\xi^5} \ , \ \tanh\bar{\alpha} = \frac{1}{\sqrt{1+\xi^2}} \simeq \frac{1}{\xi} - \frac{1}{2\xi^3} + \frac{3}{8\xi^5}, \ \mathcal{A}_0 = \frac{3}{2\zeta\xi} \tag{A21}$$

which leads to (45) with $d = 1$. Inclusion of the second term in (A5) modifies eventually $\mathcal{A}_0$ as

$$\mathcal{A}_0 = \frac{3}{2\zeta\xi} \left(1 + \frac{\xi}{6\zeta}\left(1 + \frac{\xi}{8\zeta}\right)\right) \tag{A22}$$

yielding the result displayed in (45) which extends the Ritus result for arbitrary values of ξ/ζ. We emphasize that, in the strong field regime, IPA is representative since, as stressed above, pulse shape and pulse duration effects are sub leading.

---

[1] G. A. Mourou, T. Tajima, and S. V. Bulanov, Rev. Mod. Phys. **78**, 309 (2006).

[2] A. Di Piazza, C. Müller, K. Z. Hatsagortsyan, and C. H. Keitel, Rev. Mod. Phys. **84**, 1177 (2012).

[3] G. Breit and J. A. Wheeler, Phys. Rev. **46**, 1087 (1934).

[4] H. R. Reiss, J. Math. Phys. **3**, 59 (1962).

[5] N. B. Narozhny, A. I. Nikishov, and V. I. Ritus, Sov. Phys. JETP **20**, 622 (1965).

[6] V. I. Ritus, J. Sov. Laser Res. (United States), **6:5**, 497 (1985).

[7] D. B. Blaschke, B. Kämpfer, S. M. Schmidt, A. D. Panferov, A. V. Prozorkevich, and S. A. Smolyansky, arXiv:1301.1640 [physics.plasm-ph].

[8] J. S. Schwinger, Phys. Rev. Phys. Rev. **82**, 664 (1951).

[9] G. V. Dunne, H. Gies and R. Schützhold, Phys. Rev. D **80**, 111301 (2009).

[10] F. Hebenstreit, R. Alkofer, and H. Gies, Phys. Rev. Lett. **107**, 180403 (2011).

[11] A. M. Fedotov, N. B. Narozhny, G. Mourou, and G. Korn, Phys. Rev. Lett. **105**, 080402 (2010).

[12] D. L. Burke *et al.*, Phys. Rev. Lett. **79**, 1626 (1997).

[13] V. Yanovsky *et al.*, Opt. Express **16**, 2109 (2008).

[14] `www.clf.rl.ac.uk/Facilities/Astra/Astra+Gemini/12258.aspx`

[15] `\protect\vrule width0pt\protect\href{http://www.extreme-light-infrastructure.eu}{http://w`

[16] `\protect\vrule width0pt\protect\href{http://www.hiper-laser.org/index.html}{http://www.hi`

[17] M. Boca and V. Florescu, Phys. Rev. A **80**, 053403 (2009).

[18] T. Heinzl, D. Seipt, and B. Kämpfer, Phys. Rev. A **81**, 022125 (2010).

[19] F. Mackenroth and A. Di Piazza, Phys. Rev. A **83**, 032106 (2011).

[20] D. Seipt and B. Kämpfer, Phys. Rev. A **83**, 022101 (2011).

[21] V. Dinu, T. Heinzl, and A. Ilderton, Phys. Rev. D **86**, 085037 (2012).

[22] D. Seipt and B. Kämpfer, Phys. Rev. D **85**, 101701 (2012).

[23] A. I. Titov, H. Takabe, B. Kämpfer, and A. Hosaka, Phys. Rev. Lett. **108**, 240406 (2012).

[24] T. Nousch, D. Seipt, B. Kämpfer, and A. I. Titov, Phys. Lett. B **715**, 246 (2012).

[25] K. Krajewska and J. Z. Kaminski, Phys. Rev. A **86**, 052104 (2012).

[26] S. Villalba-Chavez and C. Müller, Phys. Lett. B **718**, 992 (2013).

[27] N. V. Elkina, A. M. Fedotov, I. Y. Kostyukov, M. V. Legkov, N. B. Narozhny, E. N. Nerush, and H. Ruhl, Phys. Rev. ST Accel. Beams **14**, 054401 (2011).

[28] S. V. Bulanov *et al.*, Nucl. Instrum. Meth. A **660**, 31 (2011).

[29] F. Hebenstreit, R. Alkofer, G. V. Dunne, and H. Gies, arXiv:0910.4457 [hep-ph].

[30] F. Mackenroth, A. Di Piazza and C. H. Keitel, Phys. Rev. Lett. **105**, 063903 (2010).

[31] D. M. Volkov, Z. Phys. **94**, 250 (1935).

[32] V. B. Berestetskii, E. M. Lifshitz, and L. P. Pitaevskii, *Quantum Electrodynamics.* 2nd ed., (Course of theoretical physics; vol. 4), Oxford, New York, Pergamon Press Ltd. (1982).

[33] M. E. Grypeos, C. G. Koutroulos, V. K. Lukyanov, and A. V. Shebeko, Phys. Part. Nucl. **32**, 779 (2001) [Fiz. Elem. Chast. Atom. Yadra **32**, 1494 (2001)].

[34] G. N. Watson, A Treatise of the Theory of Bessel Functions (The University Press, Cambridge, 1944), 2nd ed.